Analytical and Bioanalytical Chemistry (2022) 414:3257–3265
https://doi.org/10.1007/s00216-022-03877-z

RESEARCH PAPER

Nanoceria-based lateral flow immunoassay for hydrogen peroxide-free colorimetric biosensing for C-reactive protein

Do Yun Kong[1] · Nam Su Heo[2] · Ji Won Kang[1] · Jin Bae Lee[2] · Hae Jin Kim[2] · Moon Il Kim[1]

Received: 1 December 2021 / Revised: 29 December 2021 / Accepted: 4 January 2022 / Published online: 14 January 2022

Abstract

During the recent several decades, lateral flow immunoassay (LFIA) constructed with gold nanoparticle (AuNP) has been widely utilized to conveniently detect target analyte. However, AuNP-based LFIA has limitations, such as limited detection sensitivity and quantification capability. Herein, to overcome these constraints, we have developed cerium oxide nanoparticle (nanoceria)-based LFIA for C-reactive protein (CRP) detection in human serum samples. It was fabricated with nanoceria, a notable nanozyme that shows an oxidase activity to quickly oxidize organic substrate, such as 3,3′,5,5′-tetramethylbenzidine (TMB), to produce colored product without any oxidizing agent (e.g., hydrogen peroxide), which is advantageous for realizing point-of-care testing (POCT) applications. By employing human blood serum spiked with CRP, the nanoceria-based LFIA showed two blue-colored lines on the test and control region within 3 min via TMB oxidation, by the captured nanoceria through antigen–antibody interaction. The produced blue-colored lines were distinguished by naked eyes and quantitated with real images acquired by a conventional smartphone with the ImageJ software. With this strategy, target CRP was specifically determined down to 117 ng mL^{-1} with high detection precisions yielding coefficient of variation of 9.8–11.3% and recovery of 90.7–103.2% using human blood serum samples. This investigation demonstrates the potential of oxidase-like nanoceria for developing LFIA, which is particularly useful in instrumentation-free POCT environments.

Keywords Lateral flow immunoassay (LFIA) · Nanoceria · Nanozyme · Oxidase-like activity · C-reactive protein

Introduction

C-reactive protein (CRP) is a pentameric acute-phase protein and generally considered as one of the most important indicators for inflammation and cardiovascular diseases such as heart attack, ischemic stroke, and coronary artery disease [1]. CRP, which is released from hepatocytes to respond to various inflammatory cytokines including tumor necrosis factor-α and interleukin-6, can provoke oxidative stress-related vascular injury [1–3]. Therefore, its physiological level is a reliable spokesperson of cardiac fitness [4]. By determining the level of CRP in human blood plasma, the early-stage diagnosis of various cardiovascular diseases is feasible [5–8]. Nowadays, the potential incidence of cardiovascular disease can be judged by the CRP concentration, at which low, average, and high risk are categorized as below 1.0 μg mL^{-1}, 1.0–3.0 μg mL^{-1}, and above 3.0 μg mL^{-1}, respectively [9]. For the quantitative determination of CRP, many interesting analytical and biosensing techniques have been developed, and among them, enzyme-linked immunosorbent assay (ELISA) based on the specific binding affinity of antibody toward CRP has been predominantly conducted [6, 10–16]. However, ELISA requires tedious experimental procedures for relatively long time by trained personnel only in laboratory environment, where expensive instrumentations are installed and utilized. Between each step of ELISA, excessive washing step is required, and if the washing was not perfectly performed, false negative or false positive

Published in the topical collection *Point-of-Care Testing* with guest editors Oliver Hayden, Peter B. Luppa, and Junhong Min.

Do Yun Kong and Nam Su Heo contributed equally to this work.

✉ Hae Jin Kim
hansol@kbsi.re.kr

✉ Moon Il Kim
moonil@gachon.ac.kr

[1] Department of BioNano Technology, Gachon University, 1342 Seongnamdae-ro, Sujeong-gu, Seongnam, Gyeonggi 13120, Republic of Korea

[2] Research Center for Materials Analysis, Korea Basic Science Institute (KBSI), Daejeon 34133, Republic of Korea

results might occur [17]. Thus, there is a great demand to develop a potent alternative enabling rapid, convenient, reliable, sensitive, and inexpensive assay for CRP.

Among assorted biosensing strategies, lateral flow immunoassay (LFIA) has been typically deployed in point-of-care testing (POCT) environment [18–20]. Target analyte can move via capillary force without any involvement of external power and be simply detected via highly specific antigen–antibody interaction presented on LFIA platform [12, 21–24]. Conventionally, LFIA is constructed with gold nanoparticle (AuNP) conjugated with antibody to obtain color responses on the designated lines generally within ~ 10 min after applying sample solution on the sample pad of LFIA strip [19]. Users can distinguish whether the target analyte is presented or not by naked eyes, based on the number of pink-colored lines. However, AuNP-based LFIA has several limitations, such as relatively low sensitivity and difficulty of reliable quantification [25–27].

Recently, enzyme-like nanomaterials (nanozymes) have been intensively studied as colorimetric probes for LFIA due to their advantageous characteristics, including high and tunable catalytic activity to produce colorimetric signal, excellent stability and robustness even in harsh conditions, and ease of mass production with low cost [23, 28, 29]. Representatively, LFIAs based on peroxidase-mimicking nanozymes, such as iron oxide magnetic nanoparticles, platinum nanoparticles, and Fe-Pt core–shell nanoparticles, were developed and successfully applied to detect clinically important analytes like the Ebola virus [20, 30, 31]. The detection was conducted through the nanozyme-mediated oxidation of colorimetric substrate, like 3,3′,5,5′-tetramethylbenzydine (TMB), consequently yielding higher sensitivity than that of conventional AuNP-based one. Although these studies demonstrate the potential of nanozyme-based LFIAs, further investigations are required to make them more suitable in practical POCT applications. In particular, since peroxidase-like nanozymes should require hydrogen peroxide (H_2O_2) as the electron acceptor for their color-generating reaction, it is unstable upon prolonged storage and, thus, may decompose and lose its ability to oxidize colorimetric substrate, resulting in reduced sensitivity and inaccurate quantification [32].

In this regard, we have developed cerium oxide nanoparticle (nanoceria)–based LFIA strip that incorporates nanoceria conjugated with CRP antibody (nanoceria@anti-CRP), to sensitively and rapidly determine CRP without the involvement of H_2O_2. Nanoceria is a unique nanozyme to exhibit oxidase-like activity that no H_2O_2 is needed to oxidize colorimetric substrate [32]. In theory, the oxidase-like activity of nanoceria has arisen from their two oxidation states, Ce^{3+} and Ce^{4+}, which generate oxygen vacancies, rendering both oxidation and reduction of nanoceria [33, 34]. Moreover, compared with other nanozymes that generally require several tens of minutes to clearly produce colorimetric responses, color generation catalyzed by nanoceria generally takes place very rapidly within a few minutes. Based on the superiorities of nanoceria, only TMB solution was added to develop blue colors on both control line (C line) and test line (T line), which was saturated within 3 min at room temperature (RT). Various characteristics of nanoceria-based LFIA for CRP detection, such as selectivity, sensitivity, and detection precision, were investigated.

Experimental section

Materials

Nanoceria, phosphate-buffered saline (PBS), sodium acetate, bovine serum albumin (BSA), human serum albumin (HSA), myoglobin, bilirubin, L-cysteine (L-Cys), L-glutamic acid (L-Glu), thrombin, TMB, 3,3′-diaminobenzidine (DAB), dimethyl sulfoxide (DMSO), ethyl alcohol, polyvinyl alcohol (PVA), and tween 20 were purchased (Sigma-Aldrich, St. Louis, MO, USA) and used as received. CRP was purchased from Fitzgerald (Acton, USA). CRP antibody (anti-CRP) and LFIA nitrocellulose pad, including goat anti-mouse IgG on C line and anti-CRP on T line, were purchased from Boreda Biotech (Seongnam, Korea). Human CRP ELISA kit was purchased from Abcam (Cambridge, UK). All solutions were prepared with deionized water purified by a Milli-Q Purification System (Millipore, USA).

Synthesis of nanoceria@anti-CRP and AuNP conjugated with CRP antibody (AuNP@anti-CRP)

To synthesize nanoceria@anti-CRP, bare nanoceria (1 ~ 10 mg mL^{-1}) was incubated with anti-CRP (50 ~ 200 μg mL^{-1}) in PBS (pH 7.4) and mixed with gentle rotation for 30 min at RT. The unreacted anti-CRP was removed by washing three times using PBS solution. Subsequently, the nanoceria conjugates were incubated for 1 h at RT in PBS buffer containing BSA at various concentrations (0 ~ 1%; w/v) to block non-specific binding at 4℃ until use. Before the real LFIA experiment, 0.1% (w/v) tween 20 was added into nanoceria@anti-CRP solution for facile movement of nanoceria@anti-CRP through the nitrocellulose membrane [20, 35]. AuNP was synthesized according to the previously reported procedures [36], and the AuNP@anti-CRP was prepared in the same procedures described above, except the utilization of AuNP rather than nanoceria.

Characterization of nanoceria and nanoceria@anti-CRP

Morphology and structure of nanoceria and nanoceria@anti-CRP were analyzed by scanning electron microscopy (SEM, Magellan 400), transmission electron microscopy (TEM, Tecnai), and field emission transmission electron microscopy (FE-TEM, Bruker, Billerica, MA, USA) with energy-dispersive X-ray spectroscopy (EDX) imaging modes. Fourier transform infrared (FT-IR, FT/IR-4600, JASCO, Easton, MD) spectra of nanoceria, nanoceria conjugated with anti-CRP without BSA treatment (nanoceria@anti-CRP w/o BSA), and nanoceria@anti-CRP were obtained from 4000 to 400 cm^{-1}. Particle size distributions of nanoceria@anti-CRP were obtained by dynamic light scattering (DLS) analysis using Zetasizer Nano-ZS (Malvern Co., Worcestershire, UK). X-ray photoelectron spectroscopy (XPS) analyses were performed using an AXIS NOVA spectrometer (KRATOS Corporation) with a monochromatic Al Kα X-ray source (150 W, 15 keV). Zeta potential analysis was performed using Zetasizer Nano-ZS (Malvern Co., Worcestershire, UK). The encapsulation yield of nanoceria@anti-CRP was calculated from the difference between the initial antibody amount and the leached amount in the supernatant by the measurement using a PierceTM bicinchoninic acid (BCA) protein assay kit (Thermo Fisher Scientific) with BSA as a standard.

Determination of oxidase-like activity of nanoceria

In a typical assay, nanoceria (1 mg mL^{-1}) in the presence (10 mM) or absence of H_2O_2 was added into a reaction buffer (sodium acetate, 0.1 M, pH 3) containing either TMB (0.5 mM) or DAB (5.0 mM). The color changes and the corresponding absorption intensities at 652 nm and 460 nm were measured using a microplate reader (Synergy H1, BioTek, VT). Steady-state kinetic assays of the nanoceria using TMB as a substrate in the absence of H_2O_2 were also performed. The concentration of nanoceria was set to 1 mg mL^{-1}, whereas the concentrations of TMB were varied. Steady-state kinetic assays of the nanoceria as peroxidase mimic, in the presence of 1 mM H_2O_2 with varied TMB or in the presence of 5 mM TMB with varied H_2O_2, were also performed. Spectroscopic measurements were conducted at 652 nm using the microplate reader, for measuring oxidized TMB. The kinetic parameters, including Michaelis–Menten constant (K_m) and maximum initial velocity (V_{max}), were obtained based on the equation $\nu = V_{max} \times 1/(K_m + [S])$, where ν is the initial velocity and $[S]$ is the concentration of substrate. The catalytic constant k_{cat} was calculated from $k_{cat} = V_{max}/[E]$, where $[E]$ is the molar concentration of nanoceria.

Determination of CRP by nanoceria- and AuNP-based LFIA

The commercial LFIA pads for CRP detection were modified to construct nanoceria-based LFIA. The conjugation pads (7 mm in width) were treated with PVA solution containing tween 20 (0.1%; w/v) overnight at RT under gentle shaking condition and dried in oven. Next, 500 µL of nanoceria@anti-CRP was dropped homogeneously on the pre-treated conjugation pads and dried at RT for 1 day in a desiccator. The treated conjugation pad and sample pad were laminated sequentially on the strip, resulting in nanoceria-based LFIA strips. AuNP-based LFIA was construed with the same procedures except that AuNP@anti-CRP was utilized rather than nanoceria@anti-CRP.

To quantitatively determine CRP using nanoceria-based LFIA, model sample solutions containing diverse concentrations of CRP were prepared in a buffer solution (PBS containing 0.15 M NaCl and 0.2% tween 20; w/v), and the prepared nanoceria-based LFIA strips were dipped into the sample solution for 10 min at RT. Next, the strips were washed 3 times by dropping sodium acetate buffer (0.1 M, pH 3), and color-generating solution containing TMB (0.5 M) in a sodium acetate buffer (0.1 M, pH 3) was dropped on the sample pad. After 3 min, the reacted strip was directly used to obtain images with a smartphone (GALAXY S8 NOTE, Samsung), followed by converting to cyan-magenta-yellow-black (CMYK) mode, which was subjected to quantitative image processing with the ImageJ software (NIH). For the quantification of CRP using AuNP-based LFIA, the color of AuNP was used to obtain images without TMB employment. For evaluating the selectivity of nanoceria-based LFIA toward target CRP, 5 µg mL^{-1} of CRP, as well as interfering substances such as human serum albumin (HSA), myoglobin (Myo), bilirubin (Bili), L-cysteine (L-Cys), L-glutamic acid (L-Glu), and thrombin (Thr), was included in the sample solutions and further processes were the same as described above.

For the determination of CRP level in human serum, original CRP level in the serum was determined using human CRP ELISA kit (Abcam). Then, pre-determined amount of CRP was spiked into serum (Sigma), followed by 100-fold diluted with PBS buffer (pH 7.4). The concentration of CRP in each spiked sample was measured using the same procedures as presented above. The recovery rate [recovery (%) = measured value/actual value × 100] and the coefficient of variation [CV (%) = SD/average × 100]

were calculated to evaluate the precision and reproducibility of the LFIA system.

Results and discussion

Construction of H_2O_2-free nanoceria-based LFIA

Nanoceria-based LFIA strip was developed for H_2O_2-free colorimetric determination of CRP in human serum. By utilizing physical interaction between nanoceria and CRP antibody, nanoceria@anti-CRP was prepared as a nanozyme probe enabling both recognition and visualization of target CRP. The prepared nanoceria@anti-CRP was physically fixed on the conjugation pad and CRP antibody and mouse IgG antibody were dispensed on T and C lines, respectively. In the presence of CRP in a sample solution, the nanoceria@anti-CRP would be captured on both lines through antigen–antibody interaction. After adding TMB solution on the sample pad, TMB would be moved by capillary force and be oxidized to produce blue color on both lines, by the high catalytic activity of captured nanoceria@anti-CRP. Importantly, nanoceria exhibits a unique oxidase-like activity to catalyze TMB oxidation without the involvement of H_2O_2, and thus, only TMB solution can be applied, which is different from the conventional peroxidase-like nanozyme probe and quite advantageous to realize practical biosensing applications. In the absence of CRP, the nanoceria@anti-CRP would be captured only on C line, and thus, only one blue line would be generated (Fig. 1). The images of resulting LFIA strip were acquired using a smartphone, and quantitative information was obtained by simple image processing with ImageJ software. We envisioned that the nanoceria-based LFIA strip would serve as an efficient biosensor capable of being used for determining CRP level in human blood in POCT environment.

The morphologies of bare nanoceria and nanoceria@anti-CRP were analyzed by TEM (Fig. 2A and 2B). TEM images showed the spherical shape of the nanoceria with a size below 5 nm. Compared with bare nanoceria, nanoceria@anti-CRP showed grey-colored region around the particles, presumably because electron beam can penetrate antibody molecules better than nanoparticles, yielding grey colors on the antibody-presenting area. The spectra of EDX proved the existence of antibodies and blocking agent (BSA) on nanoceria@anti-CRP, by observing their corresponding elements like nitrogen (N) and sulfur (S) (Figure S1). Narrow and homogeneous particle size distributions around 4 nm of bare nanoceria were observed by the DLS method (inset of Fig. 2A). Notably, nanoceria@anti-CRP retained their homogeneous nature without any aggregation during 2 days under reaction buffer, indicating its high stability sufficient for LFIA applications (Figure S2). Chemical structures of bare nanoceria, nanoceria@anti-CRP w/o BSA, and nanoceria@anti-CRP were analyzed and compared by FT-IR (Fig. 2C). Ce–O bonding was detected for all the employed samples, and as expected, amino bonding (-NH_2) as well as other bonds (C–O–C, C-O, and C-H) was detected for nanoceria@anti-CRP w/o BSA

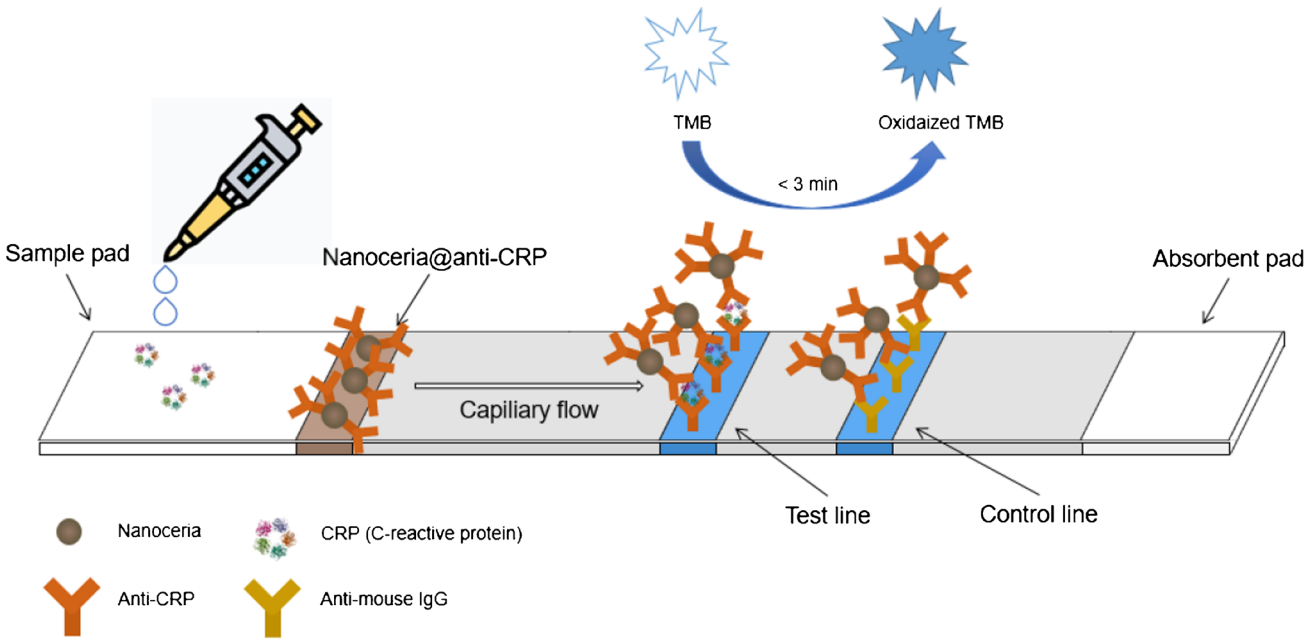

Fig. 1 Schematic illustration for nanoceria-based LFIA to detect CRP via TMB oxidation in the absence of H_2O_2

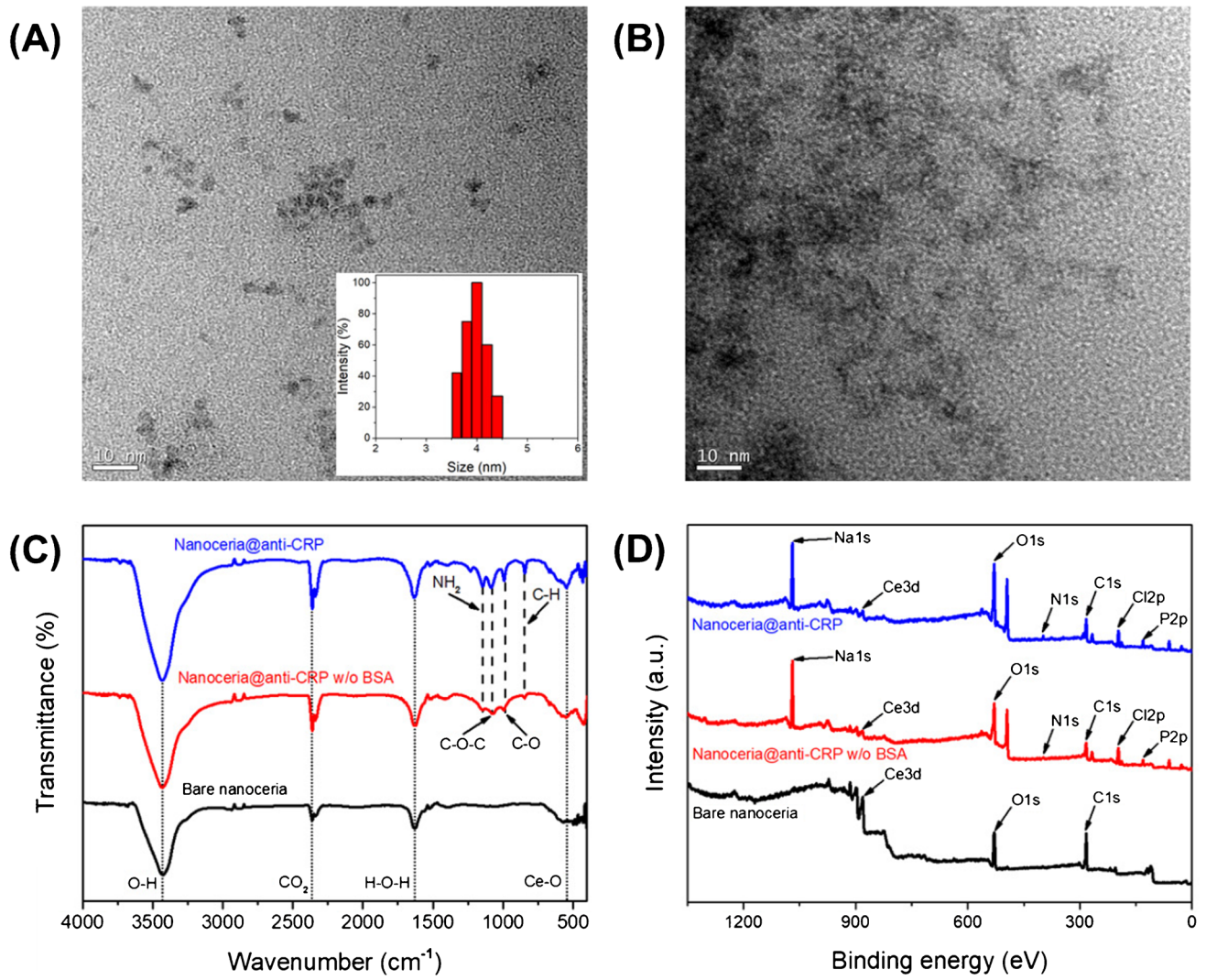

Fig. 2 Characterizations of nanoceria and nanoceria@anti-CRP. TEM images of **A** nanoceria and **B** nanoceria@anti-CRP. In the inset of (**A**), particle size distributions of nanoceria were presented. **C** FT-IR and **D** XPS spectra for nanoceria, nanoceria@anti-CRP w/o BSA, and nanoceria@anti-CRP

and nanoceria@anti-CRP, clearly showing the presence of antibodies and BSA molecules and their linkage with nanoceria [37]. Furthermore, the N1s peak in the XPS spectra of nanoceria@anti-CRP w/o BSA and nanoceria@anti-CRP confirmed the presence of protein molecules, whereas bare nanoceria did not show it (Fig. 2D). Other distinguishable Na1s and P2p peaks for nanoceria@anti-CRP w/o BSA and nanoceria@anti-CRP were originated from the utilization of PBS buffer. Surface zeta potentials of bare nanoceria and anti-CRP, dissolved in the conjugation buffer, were measured to be − 7.27 and 22.97 mV, respectively, presumably indicating that anti-CRP molecules are adsorbed on the surface of nanoceria by electrostatic interaction (Figure S3).

Oxidase-like activity of nanoceria

The oxidase-mimicking activity of nanoceria was analyzed before preparing the LFIA chip. The oxidase activity was maximized at around pH 3 (sodium acetate, 0.1 M), and thus, this buffer condition was adopted for further experiments (Figure S4). Under the typical assay conditions, the catalytic activity of nanoceria to oxidize TMB in the absence of H_2O_2 was determined to be ~ 70% to that in the presence of H_2O_2 (10 mM) (Fig. 3). With DAB as a substrate, similar high oxidation activity of nanoceria without the involvement of H_2O_2 was still observed. These results clearly showed that the nanoceria exhibited excellent activity to oxidize chromogenic substrate even in the absence of H_2O_2, although the

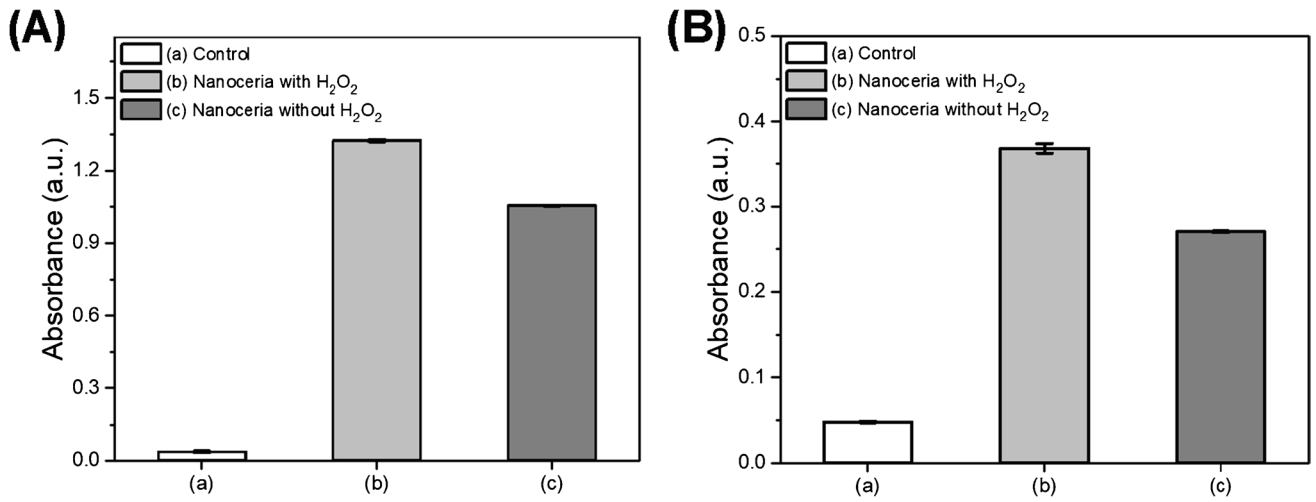

Fig. 3 Absorption intensity of **A** TMB oxidation at 652 nm and **B** DAB oxidation at 460 nm by nanoceria in the absence or presence of H_2O_2 (10 mM)

addition of H_2O_2 might help to oxidize TMB, as reported previously [32]. Although various surface modifications of nanozymes frequently yielded significantly reduced catalytic activities [38, 39], the current antibody conjugation protocol produces highly active nanoceria conjugates that retain over 80% of the original activity (Figure S5). Steady-state kinetic assays of nanoceria were next performed using TMB as a substrate to fully demonstrate the oxidase-like catalytic activity, and furthermore, the kinetic parameters as peroxidase mimic with varied TMB and H_2O_2 concentrations were evaluated and compared with those of previous studies (Table 1 and Figure S6). The results revealed that the nanoceria had excellent Michaelis–Menten constant (K_m) and catalytic constant (k_{cat}), which are among the best results of recently reported nanoceria-based nanozymes.

Determination of CRP by nanoceria-based LFIA

For developing an efficient nanoceria-based LFIA, the synthetic conditions for nanoceria@anti-CRP as well as color-generating reaction time on LFIA were optimized based on the intensity ratio (T line/C line) (Figure S7). The intensity ratio showed the highest when 5 mg mL^{-1} of nanoceria, 200 µg mL^{-1} of anti-CRP, and 0.2% (w/v) BSA were chosen and applied to prepare nanoceria@anti-CRP. Under the optimized synthetic condition, approximately the encapsulation ratio of anti-CRP was determined to be ~ 85%, measured by

Table 1 Comparison of kinetics parameters of nanoceria as oxidase or peroxidase mimic with those of previous studies

	Samples	Substrates	K_m (mM)	V_{max} (µM s^{-1})	$_{kcat}$ (s^{-1})	Ref
Oxidase	Nanoceria	TMB	0.4073	102.78	14.81	This work
	*is*PNC[(a)]		3.8	0.7	0.14	[32]
	Nanoceria		0.428	801	-	[40]
	F-capped nanoceria		0.14	6.3×10^{-2}	1.47	[41]
	CeO_2 nanorod		0.1643	8.25×10^{-3}	-	[42]
Peroxidase	Nanoceria	TMB	0.178	60.31	8.69	This work
		H_2O_2	0.132	270.63	39	
	CeO_2 nanotube	TMB	0.45	1.54×10^{-2}	1.18×10^{-3}	[43]
		H_2O_2	28.63	0.5×10^{-2}	3.85×10^{-4}	
	Pd/CeO_2 nanotube	TMB	0.39	5.94×10^{-2}	4.57×10^{-3}	[43]
		H_2O_2	9.43	1.91×10^{-2}	1.47×10^{-3}	
	PN-Ceria[(b)]	TMB	0.147	62	5.35×10^{4}	[44]
		H_2O_2	293	38	3.28×10^{4}	
	HRP	TMB	0.434	0.1	4.0×10^{3}	[45]
		H_2O_2	37	0.087	3.48×10^{3}	

[(a)] *is*PNC: In situ prepared nanoceria coated with poly(acrylic acid)

[(b)] *PN*-Ceria: Porous nanorods of ceria

triplicate BCA assays. After applying model CRP solution on sample pad, TMB solution without H_2O_2 was applied, and the effects of color-generating reaction time on assay performance were investigated. Notably, 3 min after the addition of TMB solution yielded the two clear blue lines and further reaction cannot enhance the detection performances. Thus, color-generating reaction for 3 min was chosen and utilized in further LFIA experiments. In addition, to clearly show the effects of tween 20 addition on the movement of nanoceria@anti-CRP and the corresponding CRP detection, we performed additional experiments to compare CRP detecting activities among three cases: (a) no tween 20 addition, (b) tween 20 addition into nanoceria@anti-CRP solution right before assay experiment, and (c) tween 20 addition into the storage (blocking) buffer of nanoceria@anti-CRP (Figure S8). The results show that the addition of tween 20 is essential to facilitate the movement of nanoceria@anti-CRP and generate the corresponding color signal. Furthermore, similar level of blue color intensity was produced when we added tween 20 into the nanoceria@anti-CRP solution, right before the assay experiment and just in the blocking buffer of nanoceria@anti-CRP, showing that the additional step for adding tween 20 into the nanoceria@anti-CRP solution before each assay experiment is not critically required.

Selectivity toward target CRP by nanoceria-based LFIA was first investigated. The experimental results vividly showed that our LFIA strip enabled selective determination of target CRP, whereas negligible colors were shown on T line by the negative control samples including HSA, Myo, Bili, L-Cys, L-Glu, and Thr (Fig. 4A). As the concentration of CRP increased, the color intensity ratio gradually increased via both nanoceria- and AuNP-based LFIA (Fig. 4B), yielding linear calibration plots having the equation of $y = 0.2638x + 0.1661$ and $y = 0.1496x + 0.0018$, respectively, up to ~ 10 μg mL^{-1}. Importantly, the nanoceria-based LFIA had higher slope value than that of AuNP-based one, with lower limit of detection value of 117 ng mL^{-1} than

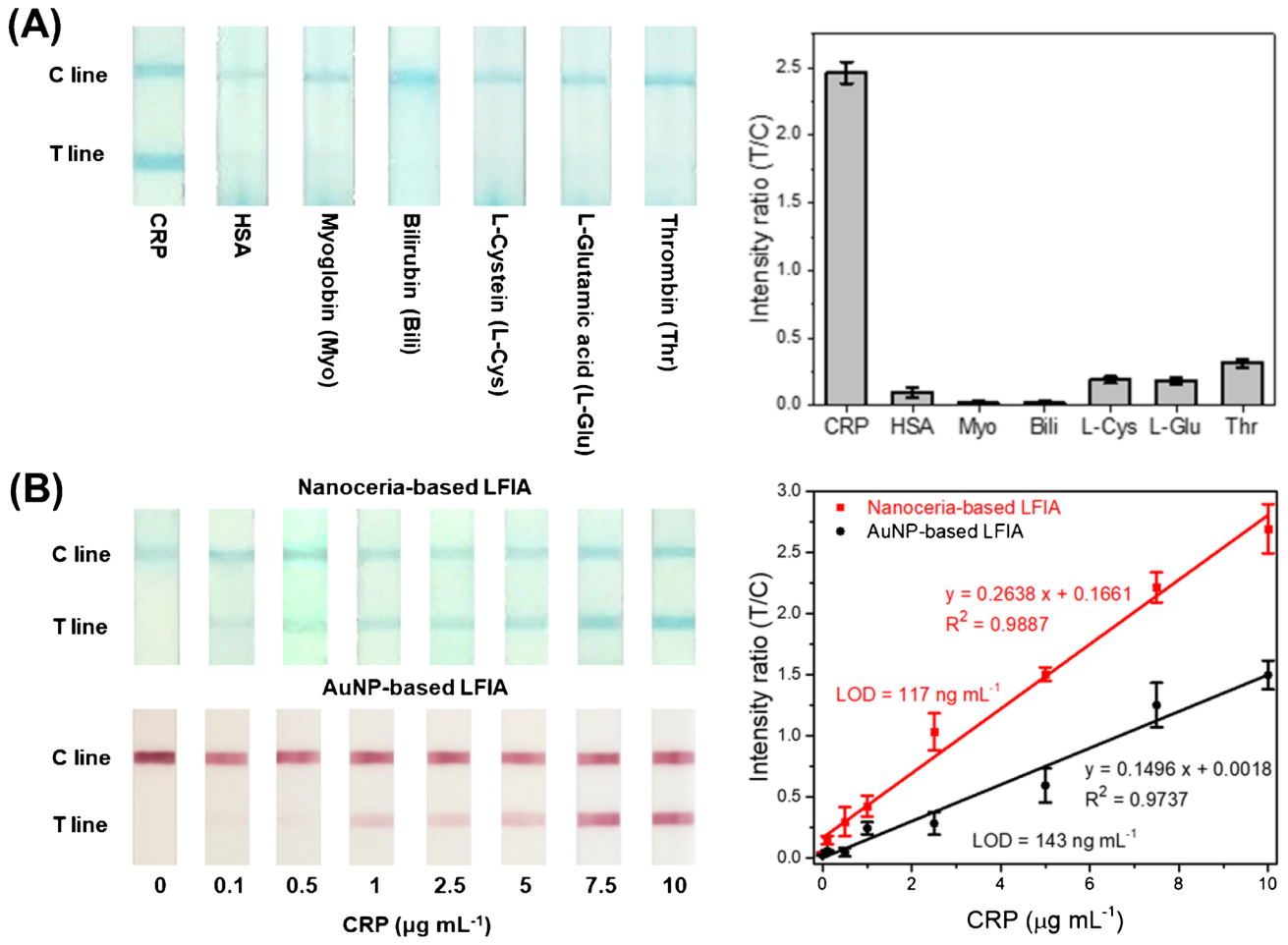

Fig. 4 **A** Real images and the corresponding intensity ratio (T line/C line) of the selective detection of CRP using nanoceria-based LFIA strip. **B** Real images and the corresponding linear calibration plot for CRP determination using nanoceria (red)- and AuNP (black)-based LFIA strip. The error bars represent the standard deviation of five independent measurements

Table 2 Detection precision of the nanoceria-based LFIA for the quantification of CRP levels in spiked human serum samples

Sample	Original amount[(a)] (μg mL^{-1})	Added (μg mL^{-1})	Expected (μg mL^{-1})	Measured[(b)] (μg mL^{-1})	SD[(c)]	CV[(d)] (%)	Recovery[(e)] (%)
Human serum	0.739	0.1	0.839	0.865	0.087	10.06	103.1
		1	1.739	1.605	0.181	11.26	92.3
		5	5.739	5.205	0.515	9.89	90.7

[(a)]Original CRP concentration in human serum was determined using human CRP ELISA kit (Abcam)

[(b)]Mean of five independent measurements

[(c)]Standard deviation of five independent measurements

[(d)]Coefficient of variation = SD/mean × 100

[(e)]Recovery = measured value/expected value × 100

that of AuNP-based one (143 ng mL^{-1}), proving high sensitivity of nanoceria-based LFIA, better than the conventional AuNP-based one and comparable with those of recent CRP detection strategies (Table S1).

Finally, we examined the diagnostic capability of the nanoceria-based LFIA strip using clinical human serum samples containing representative risk levels of CRP (low, ≤ 1 μg mL^{-1}; average, 1.0–3.0 μg mL^{-1}; and high, > 3.0 μg mL^{-1}) [9]. The original amount of CRP in the serum was first determined using a CRP ELISA kit, and a predetermined amount of CRP was added to establish the representative levels. Ten-fold dilution was applied to the prepared samples to adjust the CRP concentration within our linear range. According to the experimental results, the serum CRP levels were quantitatively determined with sufficient precision, yielding CVs ranging from 9.8 to 11.3% and recoveries ranging from 90.7 to 103.2% (Table 2), validating the excellent reproducibility and reliability of this assay. These results demonstrate that the proposed H_2O_2-free nanoceria-based LFIA strip can be employed as a promising analytical tool for convenient identification of CRP in POCT environments.

Conclusions

We herein developed a LFIA strip, where nanoceria@anti-CRP was employed as a replacement of conventional AuNP or peroxidase-like nanozyme, to rapidly, conveniently, and sensitively detect CRP. The LFIA strip displayed excellent selectivity, sensitivity, and linearity for the determination of target CRP by simply processing the real images acquired using a smartphone. The clinical utility of this LFIA strip was successfully demonstrated by reliably determining the CRP levels from clinical human serum samples. Since the nanoceria-based LFIA strip enabled rapid visual detection of the target CRP without the involvement of H_2O_2 during color-generating reaction, it should find practical applications in POCT environments. For realizing practical applications in clinical diagnostics for CRP, further analytical evaluation on real human blood samples should be preceded to directly demonstrate the clinical utility of nanoceria-based LFIA.

Supplementary Information The online version contains supplementary material available at https://doi.org/10.1007/s00216-022-03877-z.

Funding This work was supported by the National Research Foundation of Korea (NRF) grant funded by the Korean government (Ministry of Science and ICT (NRF- 2019R1A2C1087459)) and by the Gachon University research fund of 2020 (GCU-202004470001). We would like to acknowledge the financial support from the R&D Convergence Program (C 180500-KBSI).

Declarations

Conflict of interest The authors declare no competing interests.

References

1. Ridker PM, Glynn RJ, Hennekens CH. C-reactive protein adds to the predictive value of total and HDL cholesterol in determining risk of first myocardial infarction. Circulation. 1998;97(20):2007–11.
2. May A, Wang TJ. Evaluating the role of biomarkers for cardiovascular risk prediction: focus on CRP, BNP and urinary microalbumin. Expert Rev Mol Diagn. 2007;7(6):793–804.
3. Mygind ND, Harutyunyan MJ, Mathiasen AB, Ripa RS, Thune JJ, Gøtze JP, et al. The influence of statin treatment on the inflammatory biomarkers YKL-40 and HsCRP in patients with stable coronary artery disease. Inflamm Res. 2011;60(3):281–7.
4. Kuo H-K, Yen C-J, Chen J-H, Yu Y-H, Bean JF. Association of cardiorespiratory fitness and levels of C-reactive protein: data from the National Health and Nutrition Examination Survey 1999–2002. Int J Cardiol. 2007;114(1):28–33.
5. Clyne B, Olshaker JS. The C-reactive protein. J Emerg Med. 1999;17(6):1019–25.
6. Kushner I, Somerville JA. Estimation of the molecular size of C-reactive protein and C-reactive protein in serum. BBA-Protein Structure. 1970;207(1):105–14.
7. Marnell L, Mold C, Du Clos TW. C-reactive protein: ligands, receptors and role in inflammation. Clin Immunol. 2005;117(2):104–11.

8. Ridker PM. High-sensitivity C-reactive protein, inflammation, and cardiovascular risk: from concept to clinical practice to clinical benefit. Am Heart J. 2004;148(1):S19–26.
9. Kushner I, Sehgal AR. Is high-sensitivity C-reactive protein an effective screening test for cardiovascular risk? Arch Intern Med. 2002;162(8):867–9.
10. Islam MS, Kang SH. Chemiluminescence detection of label-free C-reactive protein based on catalytic activity of gold nanoparticles. Talanta. 2011;84(3):752–8.
11. Islam MS, Yu H, Lee HG, Kang SH. Molecular switching fluorescence based high sensitive detection of label-free C-reactive protein on biochip. Biosens Bioelectron. 2010;26(3):1028–35.
12. Ahn JS, Choi S, Jang SH, Chang HJ, Kim JH, Nahm KB, et al. Development of a point-of-care assay system for high-sensitivity C-reactive protein in whole blood. Clin Chim Acta. 2003;332(1–2):51–9.
13. Kim N, Kim D-K, Cho Y-J. Development of indirect-competitive quartz crystal microbalance immunosensor for C-reactive protein. Sens Actuators B Chem. 2009;143(1):444–8.
14. Choi HW, Sakata Y, Kurihara Y, Ooya T, Takeuchi T. Label-free detection of C-reactive protein using reflectometric interference spectroscopy-based sensing system. Anal Chim Acta. 2012;728:64–8.
15. Ibupoto ZH, Jamal N, Khun K, Willander M. Development of a disposable potentiometric antibody immobilized ZnO nanotubes based sensor for the detection of C-reactive protein. Sens Actuators B Chem. 2012;166:809–14.
16. Vashist SK, Czilwik G, van Oordt T, von Stetten F, Zengerle R, Schneider EM, et al. One-step kinetics-based immunoassay for the highly sensitive detection of C-reactive protein in less than 30 min. Anal Biochem. 2014;456:32–7.
17. Pearson TA, Mensah GA, Hong Y, Smith SC Jr. CDC/AHA workshop on markers of inflammation and cardiovascular disease: application to clinical and public health practice: overview. Circulation. 2004;110(25):e543–4.
18. Taranova NA, Byzova NA, Zaiko VV, Starovoitova TA, Vengerov YY, Zherdev AV, et al. Integration of lateral flow and microarray technologies for multiplex immunoassay: application to the determination of drugs of abuse. Microchim Acta. 2013;180(11–12):1165–72.
19 Nayak S, Blumenfeld NR, Laksanasopin T, Sia SK. Point-of-care diagnostics: recent developments in a connected age. Anal Chem. 2017;89(1):102–23.
20. Kim MS, Kweon SH, Cho S, An SSA, Kim MI, Doh J, et al. Pt-decorated magnetic nanozymes for facile and sensitive point-of-care bioassay. ACS Appl Mater Interfaces. 2017;9(40):35133–40.
21. Miranda OR, Li X, Garcia-Gonzalez L, Zhu Z-J, Yan B, Bunz UH, et al. Colorimetric bacteria sensing using a supramolecular enzyme–nanoparticle biosensor. J Am Chem Soc. 2011;133(25):9650–3.
22. Song Y, Wei W, Qu X. Colorimetric biosensing using smart materials. Adv Mater. 2011;23(37):4215–36.
23. Hur J, Park HG, Kim MI. Reagentless colorimetric biosensing platform based on nanoceria within an agarose gel matrix. Biosens Bioelectron. 2017;93:226–33.
24. Pu KY, Liu B. Intercalating dye harnessed cationic conjugated polymer for real-time naked-eye recognition of double-stranded DNA in serum. Adv Funct Mater. 2009;19(9):1371–8.
25. Naderi M, et al. Naked-eye detection of potassium ions in a novel gold nanoparticle aggregation-based aptasensor Spectrochim. Acta A Mol Biomol Spectrosc. 2018;195:75–83.
26. Sun M, et al. Salt-induced aggregation of gold nanoparticles for photoacoustic imaging and photothermal therapy of cancer. Nanoscale. 2016;8(8):4452–7.
27. Christau S, et al. Salt-induced aggregation of negatively charged gold nanoparticles confined in a polymer brush matrix. Macromolecules. 2017;50(18):7333–43.
28. Wei H, Wang E. Nanomaterials with enzyme-like characteristics (nanozymes): next-generation artificial enzymes. Chem Soc Rev. 2013;42(14):6060–93.
29. Shin HY, Park TJ, Kim MI. Recent research trends and future prospects in nanozymes. J. Nanomater. 2015;2015.
30. Kim M, Kim MS, Kweon SH, Jeong S, Kang MH, Kim MI, Lee J, Doh J. Simple and sensitive point-of-care bioassay system based on hierarchically structured enzyme-mimetic nanoparticles. Adv Healthcare Mater. 2015;4(9):1311–6.
31. Duan D, Fan K, Zhang D, Tan S, Liang M, Liu Y, Zhang J, Zhang P, Liu W, Qiu X, Kobinger GP, Gao GF, Yan X. Nanozyme-strip for rapid local diagnosis of Ebola. Biosens Bioelectron. 2015;74:134–41.
32. Asati A, Santra S, Kaittanis C, Nath S, Perez JM. Oxidase-like activity of polymer-coated cerium oxide nanoparticles. Angew Chem. 2009;121(13):2344–8.
33. Korsvik C, Patil S, Seal S, Self WT. Superoxide dismutase mimetic properties exhibited by vacancy engineered ceria nanoparticles. Chem Commun. 2007;10:1056–8.
34. Pirmohamed T, Dowding JM, Singh S, Wasserman B, Heckert E, Karakoti AS, et al. Nanoceria exhibit redox state-dependent catalase mimetic activity. Chem Commun. 2010;46(16):2736–8.
35. Berlina AN, et al. Quantum dot-based lateral flow immunoassay for detection of chloramphenicol in milk. Anal Bioanal Chem. 2013;405(14):4997–5000.
36. Bastús NG, Comenge J, Puntes V. Kinetically controlled seeded growth synthesis of citrate-stabilized gold nanoparticles of up to 200 nm: size focusing versus Ostwald ripening. Langmuir. 2011;27(17):11098–105.
37. Gabay C, Kushner I. Acute-phase proteins and other systemic responses to inflammation. N Engl J Med. 1999;340(6):448–54.
38. McVey C, et al. Unusual switchable peroxidase-mimicking nanozyme for the determination of proteolytic biomarker. Nano Res. 2019;12(3):509–16.
39. Das B, et al. Nanozymes in point-of-care diagnosis: an emerging futuristic approach for biosensing. Nano-Micro Lett. 2021;13(1):1–51.
40. Guo R, et al. Dual role of hydrogen peroxide on the oxidase-like activity of nanoceria and its application for colorimetric hydrogen peroxide and glucose sensing. RSC Adv. 2016;6(65):59939–45.
41. Zhao Y, et al. Fluoride-capped nanoceria as a highly efficient oxidase-mimicking nanozyme: inhibiting product adsorption and increasing oxygen vacancies. Nanoscale. 2019;11(38):17841–50.
42. Wang Y, Liang R-P, Qui J-D. Nanoceria-templated metal organic frameworks with oxidase-mimicking activity boosted by hexavalent chromium. Anal Chem. 2019;92(2):2339–46.
43. Li X, et al. Synergistically enhanced peroxidase-like activity of Pd nanoparticles dispersed on CeO_2 nanotubes and their application in colorimetric sensing of sulfhydryl compounds. J Mater Sci. 2018;53(19):13912–23.
44. Tian Z, et al. Highly sensitive and robust peroxidase-like activity of porous nanorods of ceria and their application for breast cancer detection. Biomaterials. 2015;59:116–24.
45. Gao L, et al. Intrinsic peroxidase-like activity of ferromagnetic nanoparticles. Nat Nanotechnol. 2007;2(9):577–83.